Interruption of ganglioside synthesis produces central nervous system degeneration and altered axon–glial interactions

Tadashi Yamashita*†‡, Yun-Ping Wu*†, Roger Sandhoff†§, Norbert Werth¶, Hiroki Mizukami*, Jessica M. Ellis*, Jeffrey L. Dupree‖, Rudolf Geyer**, Konrad Sandhoff¶, and Richard L. Proia*††

*Genetics of Development and Disease Branch, National Institute of Diabetes and Digestive and Kidney Diseases, National Institutes of Health, Bethesda, MD 20892; §Department of Cellular and Molecular Pathology, German Cancer Research Center, Im Neuenheimer Feld 280, 69120 Heidelberg, Germany; **Biochemisches Institut, Fachbereich Humanmedizin, Justus-Liebig-Universität Giessen, Friedrichstrasse 24, D-35392 Giessen, Germany; ‖Department of Anatomy and Neurobiology, Virginia Commonwealth University, Richmond, VA 23298; and ¶Kekulé-Institut für Organische Chemie und Biochemie, Universität Bonn, Gerhard-Domagk-Strasse 1, 53121 Bonn, Germany

Edited by Roscoe O. Brady, National Institutes of Health, Bethesda, MD, and approved January 14, 2005 (received for review October 19, 2004)

Gangliosides, which are sialylated glycosphingolipids, are the major class of glycoconjugates on neurons and carry the majority of the sialic acid within the central nervous system (CNS). To determine the role of ganglioside synthesis within the CNS, mice carrying null mutations in two critical ganglioside-specific glycosyltransferase genes, *Siat9* (encoding GM3 synthase) and *Galgt1* (encoding GM2 synthase), were generated. These double-null mice were unable to synthesize gangliosides of the ganglio-series of glycosphingolipids, which are the major ganglioside class in the CNS. Soon after weaning, viable mice developed a severe neurodegenerative disease that resulted in death. Histopathological examination revealed striking vacuolar pathology in the white matter regions of the CNS with axonal degeneration and perturbed axon–glia interactions. These results indicate that ganglioside synthesis is essential for the development of a stable CNS, possibly by means of the promotion of interactions between axon and glia.

glycosphingolipid | neurodegeneration | glycosyltransferase

Gangliosides are membrane-bound glycosphingolipids‡‡ that are composed of an oligosaccharide head structure containing one or more sialic acid residues that are attached to a ceramide lipid anchor (2). These gangliosides are abundantly expressed in the mammalian nervous system primarily as the ganglio-series of glycosphingolipids, which contain the Galβ3GalNAcβ4Galβ4Glc core structure. In fact, gangliosides are the major glycoconjugates of neurons and carry most of the sialic acid within the brain (3, 4).

Progress in understanding physiologic functions of gangliosides has been advanced by developing mice with disruptions in key glycosyltransferase genes that control the synthesis of gangliosides. For example, the *Galgt1* gene encodes GM2/GD2 synthase (UDP-*N*-acetyl-D-galactosamine:GM3/GM2/GD2 synthase, EC 2.4.1.92, also known as GalNAcT). Mice in which the *Galgt1* gene is disrupted remain viable despite a lack of complex ganglio-series gangliosides (5, 6). The brains of these mice contain large amounts of the simple gangliosides, GM3 and GD3, because of interruption of the enzymatic ganglioside synthesis pathway. Although these mice have a near-normal lifespan, they show evidence of dysmyelination and some axonal degeneration in optic and sciatic nerves (7). Furthermore, older mice with these mutations exhibit certain motor function defects (8). Mice with a disrupted *Siat8a* gene [GD3 synthase, CMP-sialic acid:GM3 α-2,8-sialyltransferase (EC 2.4.99.8)] are b-series ganglioside-deficient but show a relatively normal phenotype (9, 10). However, double-mutant mice carrying the disrupted *Galgt1* and *Siat8a* genes produce GM3 as the only major brain ganglioside. These mice have a shortened lifespan and exhibit fatal audiogenic seizures and peripheral nerve degeneration (10, 11). We recently established a line of mice with mutations in the *Siat9* gene that encodes GM3 synthase (CMP-NeuAc:lactosylceramide α-2,3-sialyltransferase; EC 2.4.99.9) (12). These *Siat9*-null mice had no overt neurologic anomalies, possibly because of diversion of the ganglioside synthesis pathway to the o-series of gangliosides (Fig. 1*A*).

Each of the ganglioside glycosyltransferase-null mice described thus far exhibit a partial disruption of ganglioside synthesis. As a result, ganglioside functions may have been masked by the redundancy of residual ganglioside structures. To totally eliminate synthesis of ganglio-series gangliosides, we derived double-null mice carrying null mutations in both the *Siat9* and *Galgt1* genes, allowing, to our knowledge for the first time, an examination of the consequences of a complete absence of these gangliosides. Although viable mice were obtained, these ganglioside-deficient mice exhibit rapid and profound neurodegeneration with severe pathology in the white matter and central nervous system (CNS) axons. These results demonstrate that gangliosides play an important role in stabilizing the maturing CNS, possibly because of the promotion of interactions between axon and glia.

Materials and Methods

Establishment of *Galgt1 Siat9* Double-Null Mice. Homozygous $Galgt1^{-/-}$ mice (6) were bred with $Siat9^{-/-}$ mice (12) to obtain double-heterozygous mice. By cross-breeding the double-heterozygotes, $Siat9^{-/-}$ $Galgt1^{-/-}$ mice were obtained. The background of the mutant mice was mixed C57BL/6 and 129/Sv strains. Mutant *Galgt1* and *Siat9* alleles were confirmed by PCR (6, 12). $Siat9^{+/+}$, $Galgt1^{+/+}$ mice littermates were used as controls for determination of body weight and brain size. All animal procedures were approved by the National Institute of Diabetes and Digestive and Kidney Diseases and were performed in accordance with the National Institutes of Health guidelines.

Histological Analysis. Animals were perfused with 4% paraformaldehyde/0.1%glutaraldehyde. Brain and spinal cord were removed and cut sagitally at the midline and processed for paraffin embedding, and sections were stained with hematoxy-

This paper was submitted directly (Track II) to the PNAS office.

Abbreviations: GFAP, glial fibrillary acidic protein; MAG, myelin-associated glycoprotein.

†T.Y., Y.-P.W., and R.S. contributed equally to this work.

‡To whom correspondence may be sent at the present address: Department of Cell Processing, Institute of Medical Science, Shirokanedai 4-6-1, Minato-ku Tokyo, 108-8639 Japan. E-mail: ty10104@ims.u-tokyo.ac.jp.

††To whom correspondence may be addressed. E-mail: proia@nih.gov.

‡‡The glycolipids nomenclature is as described by Svennerholm (1) and recommended by the International Union of Pure and Applied Chemistry [Chester, M. A. (1997) *Pure Appl. Chem.* **69,** 2475–2487].

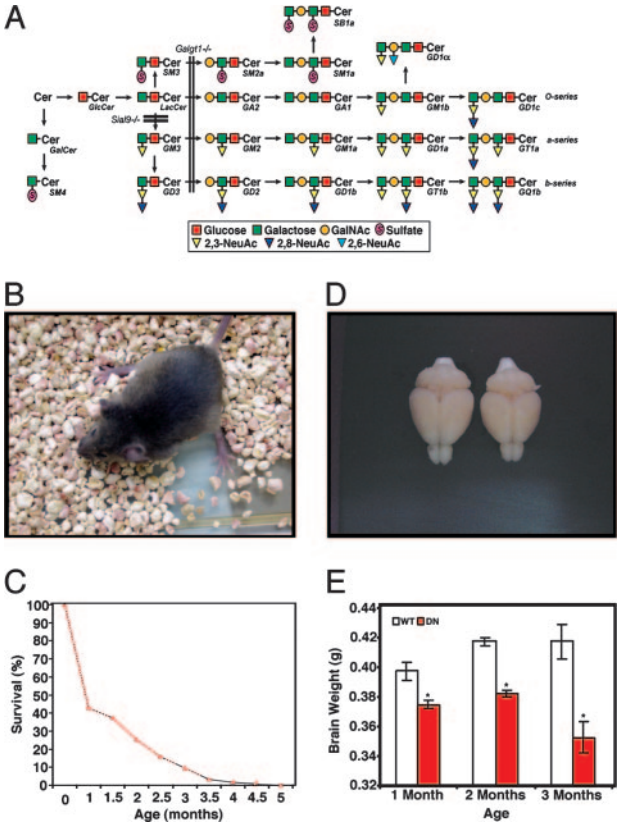

Fig. 1. Analysis of ganglioside-deficient mice. (*A*) Biosynthesis of ganglio-series glycosphingolipids. Blocks in the pathway in *Galgt1*$^{-/-}$ and *Siat9*$^{-/-}$ mice are shown. (*B*) Severe hind limb weakness in a 2.5-month-old double-null *Galgt1*$^{-/-}$ *Siat9*$^{-/-}$ mouse. (*C*) Survival of *Galgt1*$^{-/-}$ *Siat9*$^{-/-}$ mice (n = 126; males, 68; females, 58). (*D*) Gross morphology of *Galgt1*$^{-/-}$ *Siat9*$^{-/-}$ (right) and WT brains at 2.5 months of age. The brain from the double-null mouse appears smaller but morphologically intact. (*E*) Brain weight of the double-null (DN) *Galgt1*$^{-/-}$ *Siat9*$^{-/-}$ and WT mice at 1, 2, and 3 months of age (n = 4, each genotype; *, P = 0.05).

lin/eosin, Bielschowsky, Luxol fast blue, or cresyl fast violet. For immunohistochemistry, the primary antibodies used were anti-glial fibrillary acidic protein (anti-GFAP) (1:1,500 dilution; DAKO) and F4/80 (1;100; Serotec). Color visualization of the reaction product was performed with a horseradish peroxidase system (PicTure-Plus kit, Zymed, San Francisco). Slides were counterstained with acid hematoxylin or methyl green. The *in situ* Apoptosis Assay (Oncogene Science) was used to detect DNA fragmentation, according to the manufacturer's instructions. For electron microscopy, tissues were postfixed with 1% osmium tetrahydroxide and processed for embedding in plastic resin. Semithin sections then were cut and stained with toluidine blue before examination. Selected areas were further thin-sectioned, stained with uranylacetate and lead citrate, and examined under a Philips EM 410 electron microscope.

Western Blot Analysis. Brain extracts were prepared by homogenization in 50 mM Tris·HCl (pH 7.5) and 2% SDS, followed by 5 min of boiling. After centrifugation, 20 mg of homogenate protein were loaded on 4–20% Tris·glycine polyacrylamide gels (nonreducing conditions) (Invitrogen) and blotted onto nylon membranes (Invitrogen). Protein concentrations were determined by using the modified Bradford assay (Bio-Rad) with BSA as standard. The nylon blots were blocked by immersion in PBS containing 5% milk powder (Bio-Rad) and 0.05% Tween 20 for 60 min at room temperature before incubation overnight at 4°C with individual primary antibodies, including anti-myelin-associated glycoprotein (MAG) (5 μg/ml, Chemicon), anti-myelin basic protein (1 μg/ml, Pharmingen), anti-2′,3′-cyclic nucleotide 3′-phosphodiesterase (2 μg/ml, Chemicon) anti-GFAP (1:500, Santa Cruz Biotechnology), anti-phospho-extracellular signal-regulated kinase (1:500, Santa Cruz Biotechnology), anti-total extracellular signal-regulated kinase (1:500, Santa Cruz Biotechnology), or anti-β-tubulin (1:500, Santa Cruz Biotechnology). Peroxidase-conjugated anti-mouse, -goat, or -rabbit antibodies (dilutions ranging from 1:3,000 to 1:5,000, Santa Cruz Biotechnology) were used as secondary antibodies. Immunoreactivity was detected by using enhanced chemiluminescence (ECL) reagent (Amersham Pharmacia). Qualification and normalization of band intensities was performed on digital images scanned from autoradiographs.

Lipid Analysis. Lipids were isolated as described in refs. 12 and 13. Reaction mixtures used for sialidase treatment consisted of the following components in a total volume of 0.25 ml: 25 μmol of potassium acetate buffer (pH 4.5), 75 μg of BSA, 0.25 μmol of calcium chloride, 20 μg of substrate (wet weight), and 0.02 units of *Vibrio cholera* sialidase. The solution was incubated for 1 h at 37°C, and the reaction was terminated by heating for 5 min at 100°C. Desalination was performed by using RP-18 columns (14).

Lanes of a TLC plate, with solvent system CHCl/MeOH/0.22% $CaCl_2$ [60/35/8 (vol/vol/vol)], each were loaded with lipids extracted from the equivalent of 15 mg (wet weight) of brain. Ganglioside bands were detected with a phosphoric acid/copper sulfate reagent [15.6 g of CuSO4–(H_2O)5 and 9.4 ml of H_3PO_4 (85%, wt/vol) in 100 ml of H_2O]. Monosaccharide linkage analyses were performed as described in ref. 15. The TLC plate was sprayed with the reagent and developed at 160°C for 15 min, and nanoelectrospray tandem MS was performed as described in ref. 13. Sphingosine, glucosylsphingosine, (psychosine), and lactosylsphingosine were obtained from Matreya (Pleasant Gap, PA). Mass spectrometric standards for ceramide [e.g., Cer(18:1, 14:0), Cer(18:1, 19:0), and Cer(18:1, 25:0)], hexosylceramide [e.g., GlcCer(18:1, 14:0), GlcCer(18:1, 19:0), and GlcCer(18:1, 25:0)], lactosylceramide [e.g., LacCer(18:1, 14:0), LacCer(18:1, 19:0), and LacCer(18:1, 27:0)] were synthesized from sphingosine, glucosylsphingosine (psychosine), and lactosylsphingosine, respectively. Synthesis of and standardization to the sulfatide standards, SM4 and SM3, was performed as described in ref. 13. All analyses were performed with a triple quadrupole instrument (Quattro II, Micromass, Cheshire, U.K.) equipped with a nanoelectrospray source (13).

Statistical Analysis. Results are presented as means ± SD of three independent experiments. Results from experimental groups and controls were compared by Student's t test and were considered significant if two-tailed P values were <0.05.

Results

Derivation of Mice Without Ganglio-Series Gangliosides. To determine the effect of the deletion of the ganglio-series of glycosphingolipids, we derived mice simultaneously carrying a null *Galgt1* gene, which normally encodes GM2 synthase, and a null *Siat9* gene, which normally encodes GM3 synthase. Based on the glycosphingolipid biosynthetic pathway shown in Fig. 1*A*, the deletion of these two enzymes would be predicted to completely block the synthesis of gangliosides of ganglio-series of glycosphingolipids.

Viable double-mutant mice were obtained in the frequency expected by Mendelian considerations, indicating the absence of embryonic lethality. However, at 2 weeks of age, double-null mice developed hind limb weakness, ataxia, and tremors, and these abnormalities became more severe with increasing age

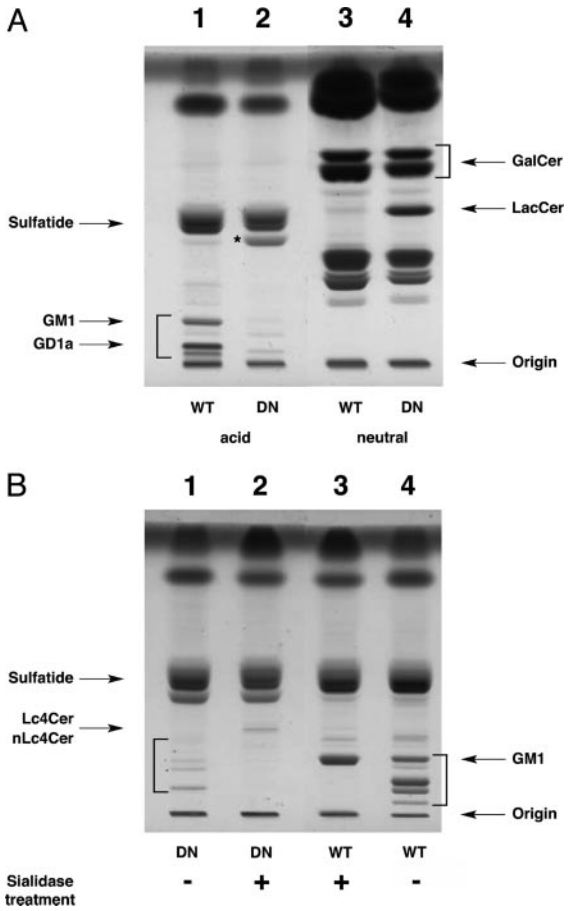

Fig. 2. Brain lipid analysis. (*A*) Acidic (lanes 1 and 2) and neutral (lanes 3 and 4) glycolipids were isolated from the brains of double-null *Galgt1*$^{-/-}$ *Siat9*$^{-/-}$ (DN, lanes 2 and 4) and WT (lanes 1 and 3) mice. The asterisk indicates the band identified as LacCerSO4. Brackets indicate normal gangliosides in lane 1. (*B*) Sialidase treatment (lanes 2 and 3) of acidic brain glycolipids from *Galgt1 Siat9* double-null (DN, lanes 1 and 2) and WT (lanes 3 and 4) mice. Brackets indicate the location of ganglioside bands in lanes 1 and 2. Upon sialidase digestion, the WT gangliosides (lane 4, bracket) were converted to GM1 (lane 3), and the double-null gangliosides (lane 1, bracket) were converted to a band migrating with Lc4Cer and nLc4Cer (lane 2). Each lane was loaded with the equivalent of 15 mg (wet weight) of homogenates.

(Fig. 1*B*). After weaning at 3 weeks, the majority of double-null mice died over the subsequent 2 months, with only rare mice surviving to 5 months of age (Fig. 1*C*). Single mutant *Galgt1*- or *Siat9*-null mice survived for >1 year and did not exhibit any neurologic abnormalities.

Lipid Analyses. TLC analysis of the acidic lipids in brains from double-null mice demonstrated absence of the major brain gangliosides species (Fig. 2*A*). However, the TLC plate also showed faint bands that did not migrate with the major ganglioside species. A major acidic lipid species (asterisk in Fig. 2*A*, lane 2) was present, which was identified by linkage analysis as lactosylceramide-3-sulfate (data not shown). The TLC neutral lipid pattern for double-null mice brains was similar to that of the wild-type (WT) brains, except for the presence of lactosylceramide as a major species (Fig. 2*A*, lane 4).

Tandem MS identified ceramide and hexosylceramide, but not lactosylceramide, in the brain glycosphingolipid extracts of WT mice (see Fig. 7*A*, which is published as supporting information on the PNAS web site). No complex sulfatides (e.g., SM3, SM2, or SB1a) were detected other than sulfatide, SM4s (galactosylceramide sulfate) (Fig. 8*A*, which is published as supporting information on the PNAS web site). In contrast to the mass spectra of brain lipids from WT mice, mass spectra from double-null *Galgt1 Siat9* mice were consistent with the presence of lactosylceramide and the complex sulfatide SM3 (lactosylceramide sulfate) (Figs. 7*B* and 8*B*). In the product ion spectra of both SM3-species (m/z 968 and 996), the following fragments indicate the presence of a sulfated lactosylceramide and suggest two different sphingosines (C18- and C20-sph): (16) (m/z 80, measured at high collision energy), $[HSO_4]^-$ (m/z 97), $[Hex\text{-}OSO_3\text{–}H_2O]^-$ (m/z 241), [stearic acid–H^+]$^-$ (m/z 283), and $[Hex_2\text{-}OSO_3\text{–}H_2O]^-$ (m/z 403).

Table 1. Sphingolipid content of WT and *Galgt1 Siat9* double-null brains

Sphingolipid	WT 1	WT 2	*Galgt1 Siat9* DN 1	*Galgt1 Siat9* DN 2
Cer	1,200	610	730	300
HexosylCer	4,400	4,700	4,700	7,600
LactosylCer	<200	<200	3,700	2,700
SM4s	2,200	2,000	2,800	2,700
SM3 (LacCer II^3-sulfate)	<40	<40	450	480

Quantitation of ceramide (Cer), hexosylceramide (HexosylCer), lactosylceramide (LactosylCer), SM4s, and SM3 in lipid extracts from two brains from WT mice (WT 1 and 2) and two brains from *Galgt1 Siat9* double-null mice (*Galgt1Siat9* DN 1 and 2). Values are in picomoles of lipid per milligram of wet weight.

Lactosylceramide and sulfated lactosylceramide (SM3) have a ceramide pattern that is composed of sphingosine with an 18- or 20-carbon chain and stearic acid (Figs. 7 *B* and *C* and 8*B*). This pattern is identical to the ceramide pattern of gangliosides from the WT mouse brain (data not shown) but is completely different from the galactosylceramide (HexCer) and sulfatide SM4 ceramide pattern of WT and double-null mice glycolipids (predominately C18-sphingosine and mainly C22- and C24-fatty acids with a high degree of α-hydroxylation) (Figs. 7 and 8). By adding internal standards before the lipid extraction, the amounts of ceramide, hexosylceramide, lactosylceramide, SM4s, and SM3 in mouse brains were quantified (Table 1). These results indicate that interruption of ganglioside synthesis in neurons in the double-mutant mice results in a shift toward synthesis of lactosylceramide and lactosylceramide-3-sulfate. However, an elevation of potentially cytotoxic ceramide was not found.

Sialidase treatment of the acidic lipid fraction of WT mice resulted in conversion of the major ganglioside species to the mono-sialyl ganglioside GM1 (Fig. 2*B*, lanes 3 and 4). In the double-null mice, the faint bands in this region were converted by sialidase to a band that was distinct from GM1 and that had mobility similar to neolactotetraosylceramide (nLc4Cer) and lactotetraosylceramide (Lc4Cer) (Fig. 2*B*, lanes 1 and 2). This sialidase-treated material was subjected to MS analysis, which demonstrated the presence of a tetraosylceramide with the structure Cer–Hex–Hex–HexNAc–Hex. Because its product ion spectra was different from that of gangliotetraosylceramide (Gg4Cer) (data not shown), the lipid must correspond to Lc4Cer or to nLc4Cer. Monosaccharide linkage analysis and MS fragment pattern identified this lipid as nLc4Cer (data not shown). These data indicate that gangliosides of the neolacto series were present at low levels in the double-null mice.

CNS Degeneration in the Absence of Gangliosides. At 1 month of age, the brains of the double-mutant mice were morphologically intact but were slightly smaller than those of WT mice (Fig. 1 *D* and *E*). The brains of the double-null mice showed a progressive decrease in size between 2 and 3 months of age, suggesting a severe neurodegenerative process (Fig. 1*E*). At 1 month of age,

BIOCHEMISTRY

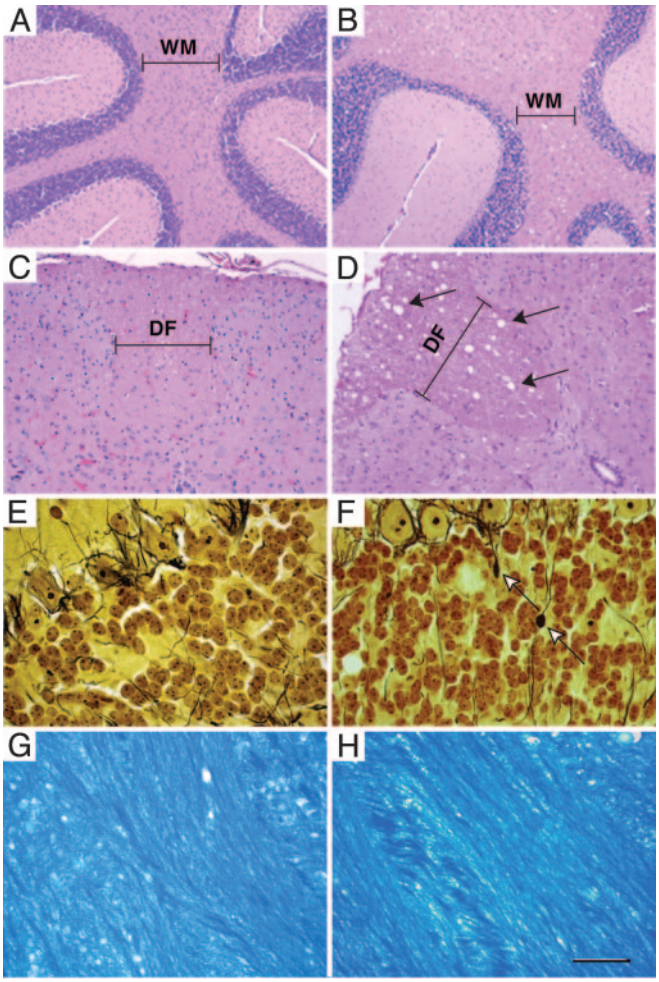

Fig. 3. CNS pathology in *Galgt1 Siat9* double-null mice. Tissue sections from WT (*A*, *C*, *E*, and *G*) and double-null (*B*, *D*, *F*, and *H*) mice are shown. (*A* and *B*) Hematoxylin/eosin-stained sections of the cerebellum from 2.5-month-old mice. Note the vacuoles in the white matter (WM) area of the double-null mice. (Bars: 100 μm.) (*C* and *D*) Hematoxylin/eosin-stained sections of the spinal cord from 5-month-old mice. Note the vacuoles (arrows) in the white-matter area (dorsal funiculus; DF) of the double-null mice. (Bars: 40 μm.) (*E* and *F*) Silver-stained sections of the cerebellum from 2.5-month-old mice. Note the axonal spheroids (arrows) in the double-null mice. (Bars: 20 μm.) (*G* and *H*) Luxol Fast Blue staining of the corpus callosum region shows that the degree of myelination is similar in WT and double-null mice. (Bars: 20 μm.)

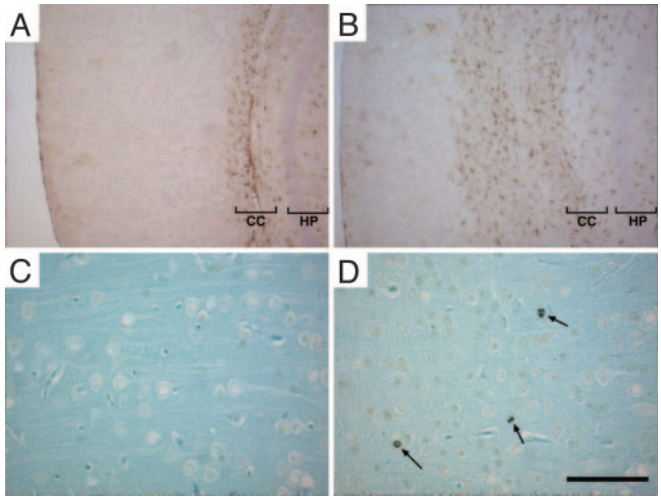

Fig. 4. Apoptosis and astrogliosis in *Galgt1 Siat9* double-null mice. Results from WT (*A* and *C*) and *Galgt1 Siat9* double-null (*B* and *D*) mice are shown. (*A* and *B*) Sections stained with anti-GFAP antibody. Note the extensive staining (brown) in cortex region adjacent to the corpus callosum (CC) in the double-null brain. HP, hippocampus. (Bars: 100 μm.) (*C* and *D*) TUNEL staining of the cerebral cortex showing apoptotic cells (arrows) in the section from the double-null mice. (Bars: 20 μm.)

histologic evaluation revealed striking vacuolization in the spinal and cerebellar white matter (Fig. 3 *A–D*) and in the brainstem fiber tracts (data not shown). The vacuolization became more prominent, especially in regions of white matter, as the double-null mice aged. Generalized myelination, as determined with Luxol Fast Blue staining, was similar when comparing WT and double-null mice (Fig. 3 *G* and *H*). Axonal spheroid formation, often associated with neurodegenerative processes (17), was observed in the cerebellar white matter and granular layers (Fig. 3 *E* and *F*; see also Fig. 5*D*, asterisk). Immunohistochemical staining with an anti-GFAP antibody demonstrated an astrocytic response in the brains of the double-null mice, especially in the surrounding white matter regions (Fig. 4 *A* and *B*). Densely staining astrocytes were prominent around the corpus callosum and in the white matter tract of the cerebellum. Enhanced staining was also seen within the cerebellar molecular layer (data not shown). Western blot analysis demonstrated enhanced expression of GFAP in the brains of the double-null mice (Fig. 6 *D* and *H*), and CNS degeneration was corroborated by the detection of apoptotic cells in the cerebral cortex (Fig. 4 *C* and *D*).

Electron micrographic analysis revealed marked degeneration of myelinated axons in double-null mice (Fig. 5 *A*, *B*, and *D*). Tubulovesicular structures, which have been described in various pathological conditions and are believed to represent a stage of axonal degeneration (18), were observed in the cerebellar axons (Fig. 5*B*). Interestingly, oligodendrocytes, identified by the presence of microtubules, contained massive cytoplasmic vacuoles (Fig. 5 *C* and *D*). Abnormalities of paranodal junctions at the node of Ranvier were detected in double-null mice, indicating possible impairment of axonal–glial interactions (19, 20). Paranode loops that faced away from the axon (Fig. 5 *E* and *F*) also were observed. Additionally, transverse bands, which are normally present in regularly arrayed electron densities in the periaxonal space, were not properly formed.

Western blot analysis of myelin proteins revealed that MAG, myelin basic protein, and 2′,3′-cyclic nucleotide 3′-phosphodiesterase were present in similar amounts when comparing brains from young double-null and young WT mice (Fig. 6 *A–C*). These data, along with the normal level of myelin lipids, galactosylceramide, and SM4s observed in initial experiments (Table 1), suggest that oligodendrocyte differentiation proceeds normally in double-null mice.

Discussion

The present study demonstrated that simultaneous disruption of the genes encoding GM3 and GM2 synthase blocked the synthesis of gangliosides of the ganglio-series of glycosphingolipids and resulted in abnormally high levels of lactosylceramide and lactosylceramide-3-sulfate, which is consistent with predictions based on the biosynthetic pathway (Fig. 1*A*). Given the similarity in the ceramide moiety, the lactosylceramides presumably were produced by neurons, which also produce the bulk of the gangliosides. Relatively low levels of a different ganglioside series, neolacto, were detected in the brains of the double-null mice. These neolacto-series gangliosides have been previously characterized as normal constituents of the human CNS (21).

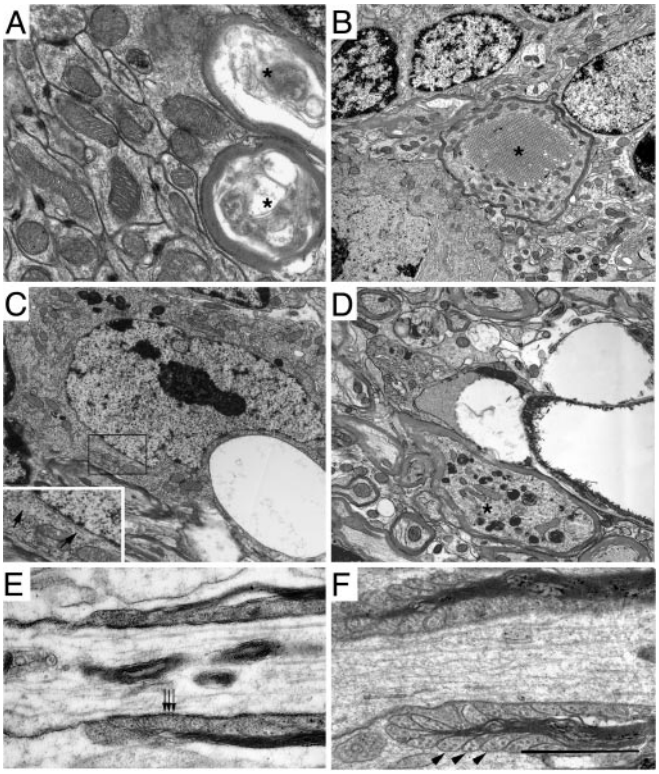

Fig. 5. Axonal degeneration, vacuolated oligodendrocytes, and abnormal axon–glia interactions in *Galgt1 Siat9* double-null mice. (*A–D*) Electron micrographs of the cerebellum from 3-month-old double-null mice. (*A* and *B*) Axonal degeneration in double-null mice. The marked degeneration of myelinated axons is indicated by asterisks in *A*. Tubulovesicular structures in a myelinated axon are noted by asterisks in *B*. Note the irregular myelin. (*C* and *D*) Abnormal oligodendrocytes in double-null mice. Note the large vacuoles in the cytoplasm of oligodendrocytes. The arrows (*C Inset*) indicate the microtubules of the oligodendrocyte. Asterisk in *D* indicates axonal spheroids. (*E* and *F*) Perturbation of the paranodal organization of double-null mice. Electron micrographs of the spinal cord of the paranodal region in WT (*E*) and double-null (*F*) mice at 1.5 months of age. In *E*, the paranodal loops are tightly opposed to the axon, and the characteristic transverse bands are also apparent (arrows). *F* shows reversed paranodal loops (arrowheads) that face away from the axon with no transverse bands. (Bars: *A*, 2 μm; *B* and *C*, 6 μm; *E* and *F*, 1 μm.)

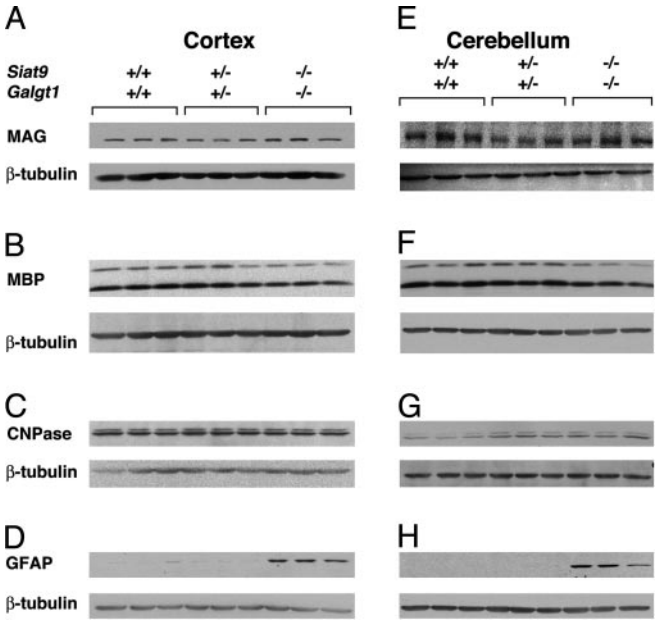

Fig. 6. Western blot analysis of oligodendrocyte and astrocyte proteins. Analysis was performed by using cerebral cortex and cerebellum lysates from the indicated genotypes at 3 months of age. Western blot analyses of MAG (*A* and *E*), myelin basic protein (MBP) (*B* and *F*), 2′,3′-cyclic nucleotide 3′-phosphodiesterase (CNPase) (*C* and *G*), and GFAP (*D* and *H*) are shown. In each case, the same blot was stripped and reprobed for β-tubulin as a loading control.

Mice with totally deficient ganglio-series ganglioside synthesis were born without gross abnormalities and with a morphologically intact CNS. The striking changes in content and composition of gangliosides during embryonic brain development (22) suggest that that these glycoconjugates may be essential for development. However, the present study indicates that synthesis of the ganglio-series gangliosides is not required for embryonic neuronal development and morphogenesis of the brain.

In contrast to the relatively subtle phenotypes of mice with single deletions of glycosyltransferase genes, double-null mice displayed a lethal phenotype. Neurologic abnormalities were noted soon after birth and included tremors and weakened hind limbs with uncoordinated gait; these mice failed to thrive and typically died soon after weaning. The presence of a catastrophic neurodegenerative process was corroborated by shrinkage of the brain, apoptosis in the cerebral cortex, astrogliosis, and vacuolar pathology in white-matter areas, particularly in the oligodendrocytes. Severe axonal disturbances were reflected by the presence of axonal spheroids and by ultrastructural evidence of axonal degeneration. Furthermore, electron microscopy demonstrated paranodal loops of myelin in the node of Ranvier that were not tightly associated with the axonal membrane, indicating abnormal axon–glial interactions in the double-null mice that may subsequently lead to axonal degeneration and disturbances of oligodendrocytes.

The interruption of ganglioside synthesis may interfere with axon–glial interactions by means of several mechanisms. Neuronal gangliosides mediate communication between axons and myelin-producing cells (23–25). MAG, a myelin-associated protein found on the myelin membrane adjacent to the axon, interacts with neuronal gangliosides to stabilize axonal–myelin interactions. The normal functional ligands for MAG include the complex gangliosides GD1a and GT1b (3). Aged single-null *Galgt1* mice, which lack complex gangliosides but still retain large amounts of the simple gangliosides GD3 and GM3 (5, 6), exhibit axonal degeneration and dysmyelination with accompanying motor behavioral deficits. The relatively mild phenotype of the *Galgt1* mice compared with the double-null mice may be a consequence of simple gangliosides functioning as MAG-binding partners. Indeed, GM3 ganglioside is a weak ligand for MAG (26). In contrast, double-null mice lack both simple and complex gangliosides and, therefore, do not possess any functional binding partners for MAG. Gangliosides also may participate in the organization of membrane domains on axons (27, 28) and direct adhesion receptors to discrete areas for optimal interaction with the opposing myelin membrane. Furthermore, elevated levels of lactosylceramides with the concomitant reduction of gangliosides may alter plasma membrane organization and cellular activities, as described in refs. 29–31.

Deletion of members of the gala-series of glycosphingolipids, which include galacosylceramide and sulfatide, produce mice with phenotypes remarkably similar to the double-null *Galgt1 Siat9* mice (16, 32). Furthermore, these glycolipids play key roles in axonal–glia interactions and in formation of the node of Ranvier (33). Interestingly, whereas gangliosides are produced most prominently in neurons, production of the gala-series is largely restricted to myelin-producing cells. This finding suggests that the ganglio- and gala-series of glycosphingolipids may play

parallel roles in promoting axonal–glial interactions, which is consistent with observations that concomitant deletion of gala-series glycosphingolipids and MAG genes in mice produces a more severe phenotype (34).

In conclusion, the present study demonstrates that ganglioside synthesis is required for stability of the maturing nervous system in mice and that mutations affecting ganglioside synthesis result in development of neurodegenerative disease. Indeed, recent studies have characterized a mutation in GM3 synthase in humans that suffer from epilepsy with an apparent neurodegenerative course (35).

This work was supported in part by the Humboldt Foundation (Max Planck Award) and Deutsche Forschungsgemeinschaft Grant SFB 645 (to K.S.).

1. Svennerholm, L. (1963) *J. Neurochem.* **10,** 455–463.
2. Kolter, T., Proia, R. L. & Sandhoff, K. (2002) *J. Biol. Chem.* **277,** 25859–25862.
3. Vyas, A. A. & Schnaar, R. L. (2001) *Biochimie* **83,** 677–682.
4. Tettamanti, G., Bonali, F., Marchesini, S. & Zambotti, V. (1973) *Biochim. Biophys. Acta* **296,** 160–170.
5. Takamiya, K., Yamamoto, A., Furukawa, K., Yamashiro, S., Shin, M., Okada, M., Fukumoto, S., Haraguchi, M., Takeda, N., Fujimura, K., *et al.* (1996) *Proc. Natl. Acad. Sci. USA* **93,** 10662–10667.
6. Liu, Y., Wada, R., Kawai, H., Sango, K., Deng, C., Tai, T., McDonald, M. P., Araujo, K., Crawley, J. N., Bierfreund, U., *et al.* (1999) *J. Clin. Invest.* **103,** 497–505.
7. Sheikh, K. A., Sun, J., Liu, Y., Kawai, H., Crawford, T. O., Proia, R. L., Griffin, J. W. & Schnaar, R. L. (1999) *Proc. Natl. Acad. Sci. USA* **96,** 7532–7537.
8. Chiavegatto, S., Sun, J., Nelson, R. J. & Schnaar, R. L. (2000) *Exp. Neurol.* **166,** 227–234.
9. Okada, M., Itoh Mi, M., Haraguchi, M., Okajima, T., Inoue, M., Oishi, H., Matsuda, Y., Iwamoto, T., Kawano, T., Fukumoto, S., *et al.* (2002) *J. Biol. Chem.* **277,** 1633–1636.
10. Kawai, H., Allende, M. L., Wada, R., Kono, M., Sango, K., Deng, C., Miyakawa, T., Crawley, J. N., Werth, N., Bierfreund, U., *et al.* (2001) *J. Biol. Chem.* **276,** 6885–6888.
11. Inoue, M., Fujii, Y., Furukawa, K., Okada, M., Okumura, K., Hayakawa, T. & Sugiura, Y. (2002) *J. Biol. Chem.* **277,** 29881–29888.
12. Yamashita, T., Hashiramoto, A., Haluzik, M., Mizukami, H., Beck, S., Norton, A., Kono, M., Tsuji, S., Daniotti, J. L., Werth, N., *et al.* (2003) *Proc. Natl. Acad. Sci. USA* **100,** 3445–3449.
13. Sandhoff, R., Hepbildikler, S. T., Jennemann, R., Geyer, R., Gieselmann, V., Proia, R. L., Wiegandt, H. & Grone, H. J. (2002) *J. Biol. Chem.* **277,** 20386–20398.
14. Williams, M. A. & McCluer, R. H. (1980) *J. Neurochem.* **35,** 266–269.
15. Geyer, R. & Geyer, H. (1994) *Methods Enzymol.* **230,** 86–108.
16. Honke, K., Hirahara, Y., Dupree, J., Suzuki, K., Popko, B., Fukushima, K., Fukushima, J., Nagasawa, T., Yoshida, N., Wada, Y. & Taniguchi, N. (2002) *Proc. Natl. Acad. Sci. USA* **99,** 4227–4232.
17. Aicardi, J. & Castelein, P. (1979) *Brain* **102,** 727–748.
18. Taniike, M., Mohri, I., Eguchi, N., Beuckmann, C. T., Suzuki, K. & Urade, Y. (2002) *J. Neurosci.* **22,** 4885–4896.
19. Poliak, S. & Peles, E. (2003) *Nat. Rev. Neurosci.* **4,** 968–980.
20. Popko, B. (2000) *Glia* **29,** 149–153.
21. Svennerholm, L., Bostrom, K., Fredman, P., Mansson, J. E., Rosengren, B. & Rynmark, B. M. (1989) *Biochim. Biophys. Acta* **1005,** 109–117.
22. Yu, R. K., Bieberich, E., Xia, T. & Zeng, G. (2004) *J. Lipid Res.* **45,** 783–793.
23. Vyas, A. A., Patel, H. V., Fromholt, S. E., Heffer-Lauc, M., Vyas, K. A., Dang, J., Schachner, M. & Schnaar, R. L. (2002) *Proc. Natl. Acad. Sci. USA* **99,** 8412–8417.
24. Yang, L. J., Zeller, C. B., Shaper, N. L., Kiso, M., Hasegawa, A., Shapiro, R. E. & Schnaar, R. L. (1996) *Proc. Natl. Acad. Sci. USA* **93,** 814–818.
25. Yamashita, T., Higuchi, H. & Tohyama, M. (2002) *J. Cell Biol.* **157,** 565–570.
26. Collins, B. E., Yang, L. J., Mukhopadhyay, G., Filbin, M. T., Kiso, M., Hasegawa, A. & Schnaar, R. L. (1997) *J. Biol. Chem.* **272,** 1248–1255.
27. Hakomori, S. (2004) *Glycoconj. J.* **21,** 125–137.
28. Kasahara, K., Watanabe, K., Takeuchi, K., Kaneko, H., Oohira, A., Yamamoto, T. & Sanai, Y. (2000) *J. Biol. Chem.* **275,** 34701–34709.
29. Uemura, S., Kabayama, K., Noguchi, M., Igarashi, Y. & Inokuchi, J. (2003) *Glycobiology* **13,** 207–216.
30. Inokuchi, J., Kabayama, K., Uemura, S. & Igarashi, Y. (2004) *Glycoconj. J.* **20,** 169–178.
31. Kabayama, K., Ito, N., Honke, K., Igarashi, Y. & Inokuchi, J. (2001) *J. Biol. Chem.* **276,** 26777–26783.
32. Coetzee, T., Fujita, N., Dupree, J., Shi, R., Blight, A., Suzuki, K. & Popko, B. (1996) *Cell* **86,** 209–219.
33. Dupree, J. L., Girault, J. A. & Popko, B. (1999) *J. Cell Biol.* **147,** 1145–1152.
34. Marcus, J., Dupree, J. L. & Popko, B. (2002) *J. Cell Biol.* **156,** 567–577.
35. Simpson, M. A., Cross, H., Proukakis, C., Priestman, D. A., Neville, D. C., Reinkensmeier, G., Wang, H., Wiznitzer, M., Gurtz, K., Verganelaki, A., *et al.* (2004) *Nat. Genet.* **36,** 1225–1229.